Failure Analysis of Abutment-Loaded Underground Coal Mine Stoppings during Explosion

Kutay E. Karadeniz[1]; Dogukan Guner[2]; and Taghi Sherizadeh[3]

Abstract: Underground mine structures like mine seals or built-in-place (BIP) refuge alternatives (RA) are exposed to specific loadings like explosions because of overlying and underlying strata conditions. Previous studies worked on the vertical loading response of structures like abutments from panel extraction but not the explosion resistance upon being subjected to these vertical strata loads. In this study, two steel-reinforced concrete wall designs as seal and RA applications are simulated to examine the performance and failure analysis under abutment-loading conditions during an explosion for a coal mine model using dynamic analysis by a distinct element code (3DEC). The available abutment monitoring data by longwall stoppings was used to estimate the abutment-loading conditions. The model setup was calibrated through two validation stages: (1) the concrete wall simulation with the explosion test of steel-reinforced concrete mine seal conducted by previous researchers; and (2) the stress change at the strata by the tailgate convergence-abutment-load multiplier curve. The calibrated models are subjected to various dynamic loadings to simulate explosions. The findings demonstrate that, in addition to magnitude, the pressure versus time mode of loading significantly influences the wall response. Instantaneous loading criteria can provide more cautious measurements to assess how well such walls operate in similar situations. Except for a few cases, the deformations after a single explosion are more pronounced for the effects of subsequent second and third explosions. As a result, the changes in deformation during subsequent explosions are relatively minor compared with the initial permanent deflections. **DOI: 10.1061/IJGNAI.GMENG-9285**. © *2024 American Society of Civil Engineers*.

Author keywords: Underground mining; Built-in-place refuge alternatives (RA); Mine seal; Coal mine stopping; Abutment stress.

Introduction

In many countries, mine ventilation and mine emergency plans require some underground coal mine structures to provide and sustain a safe working area. Therefore, underground coal mine stoppings have crucial impacts on the miners' health and safety; a ventilation plan and isolation of some specific areas are essential to protect miners from various hazards. Ventilation plans deemed seals (Sapko et al. 2005) and built-in-place (BIP) refuge alternatives (RA) are required by mine emergency plans to protect against some accidents like explosions.

Mine seals are used to separate active working and abandoned mining areas. From a safety perspective, their primary goal is to stop methane gas seeping from coal seams in the abandoned region from entering the working areas. They are also built to withstand blast pressures from a coal dust explosion or a potential inadvertent detonation of the trapped gas (Zipf et al. 2007). However, the main function of an RA, including mobile and BIP, is to offer a safe haven for miners who are unable to leave their working location because of dangerous gases or a blocked escape path immediately following an explosion. These underground coal mine structures are very similar since existing BIP RA designs are immobile and impractical to move regularly, making them resemble seals (Trackemas et al. 2015: Karadeniz et al. 2022). Panel seals, district seals, and crosscut seals are the three categories in that seals are divided based on where they are located within the mining layout. Panel seals are built to separate each fully extracted individual room and pillar panel or longwall panel. District seals, conversely, are designed to isolate a cluster of fully extracted panels from the ventilation system. Crosscut seals are typically constructed at the crosscuts of longwall gateroads to provide immediate sealing for the panel (Zipf et al. 2007). The detailed description and their positions in the mining layout are presented by Zipf et al. (2007). The possibility of explosive loading, roof-to-floor convergence, and air leakage are just a few factors that seal design engineers should consider for each application (Zipf et al. 2007; Trackemas et al. 2015; Kallu 2009). However, according to Zipf et al. (2007), crosscut seals tend to have strong convergence and a significant leakage potential owing to severe convergence damage near mined-out areas.

Any potential change in the overlying like softening and other structural alterations such as those caused by an increase in abutment or vertical loading based on coal panel extraction is crucial for the structural design of such underground mine stoppings (Verne et al. 2012; Mutton and Salu 2013). Considering the overlying strata, the conditions of the ribs, roof, and floor are critical in terms of convergence and subsequently impact the explosion resistance of the structure. (Sapko et al. 2005). There are two types of loads imposed on longwall pillars in the interest of the overlying strata in coal mining: Development load, which exists before

[1]Ph.D. Student, Graduate Research Assistant, Dept. of Mining and Explosives Engineering, Missouri Univ. of Science and Technology, 324 McNutt Hall, 1400 N. Bishop Ave., Rolla, MO 65409; Dept. of Mining Engineering, Middle East Technical Univ., 311, Ankara 06800, Turkey. Email: kutaykaradeniz@mst.edu; kkutay@metu.edu.tr

[2]Postdoctoral Fellow, Dept. of Mining and Explosives Engineering, 324 McNutt Hall, 1400 N. Bishop Ave., Rolla, MO 65409. ORCID: https://orcid.org/0000-0001-5704-9225. Email: dguner@mst.edu

[3]Assistant Professor, Dept. of Mining and Explosives Engineering, 324 McNutt Hall, 1400 N. Bishop Ave., Rolla, MO 65409 (corresponding author). ORCID: https://orcid.org/0000-0002-6975-317X. Email: sherizadeh@mst.edu

Note. This manuscript was submitted on June 4, 2023; approved on December 14, 2023; published online on March 29, 2024. Discussion period open until August 29, 2024; separate discussions must be submitted for individual papers. This paper is part of the ***International Journal of Geomechanics***, © ASCE, ISSN 1532-3641.

longwall mining, and abutment-load, which happens during longwall panel extraction (Mark 1990, 2006).

According to Gallagher (2005), typically, the mine is responsible for determining, specifying, and putting in any extra ground support needed to safeguard the structure after it has been installed. The secondary support requirements must, in particular, take into account the effects of longwall mining, the stability of the opening, the protection of the structure against convergence, the protection of the ribs near the seal, and the protection of mine personnel from seal failure/toppling. When poor rib conditions arise, additional rib sealing increments may be needed. These may be accomplished through grouting, the use of polyurethane foam, or the shuttering and forming of the ribs with subsequent drilling and pressure grouting. Therefore, Humphries (1999) also indicates that it is also necessary to estimate the structure's potential load from longwall abutment-loading. Also, Michael and Mutton (2017) state many design variables that influence the efficacy of the structure, one of them being the changing of loads depending on the adjacent extraction, which is difficult to define quantitatively. How structures react to explosions is crucial, hence various methods have been used to comprehend how structures deform. Analytical, experimental, and numerical research may be included in these methodologies. It is possible to assess the underground structure's level of damage and resistance to explosion blast pressures after an explosion. Observing the deformation process throughout the experiment, though, can be expensive or dangerous. Because of this, a lot of researchers prefer to use dynamic numerical methods to extrapolate and interpolate mechanisms like explosion, rock fragmentation, flyrock, and dynamic damage by water-inrush (Chen et al. 2022; Ning et al. 2022; Gai et al. 2023).

In this study, seal and BIP RA steel-reinforced concrete structures are examined by numerical simulations using a distinct element code (DEC) called 3DEC (Itasca 2021). Two different wall designs are handled to exhibit their performance and failure analysis under various abutment-loading and explosion impact conditions in a coal mine model. One of the concrete walls is the simulation of the structure used in the experimental study conducted by Zipf et al. (2009) at the National Institute for Occupational Safety and Health (NIOSH) Lake Lynn Laboratory used for several structural tests. The second structure to be analyzed is NIOSH's recommended BIP RA design (Trackemas et al. 2015). The main purpose of this study is to reveal the effects of wall deformation with changes in vertical loading conditions during panel extraction by implementing different convergence levels. This study also aims to identify quantitative changes in the deformation of the concrete wall during various mine explosion scenarios and compare the explosion resistances of two different reinforced concrete wall models. The simulated coal mine environment belongs to the Pittsburgh coal seam, considered one of the most valuable mineral resources in the United States. Accordingly, the abutment-loading conditions were successfully simulated by the quantitative study of convergence experienced by longwall stoppings, the data provided by Oyler et al. (2001) would be useful for further studies under different situations. The outcomes of the study reflected that the abutment-loading significantly changes the structural integrity of such structures. After a certain level of roof-to-floor convergence, the structures show deformation at the center before being subjected to any explosion impact. The currently used analytical solutions provide a guide to assess these structures after explosion considering central deflection with a rotation from the top; however, these structures get deformed with the increase in the vertical stress by the nature of the mining method. Therefore, it is suggested to take into consideration their vertical loading resistance in the current assessments. This study can help improve these assessments by being a reference line and reflecting a need for further studies on this effect of increasing vertical stress.

Methodology

This study mainly integrates field studies, experimental work, and numerical setups. Validation is regarded as a metric of model accuracy between model predictions and the real world in numerical models for consequence analysis. When measurements of a quantity of interest are compared with model predictions of that quantity, experiments represent the real world in this sense. The basis for model validation is the degree of agreement between the experiment and model prediction, which is regarded as a measure of model accuracy (Borg et al. 2014). Therefore, to be confident in the outcomes of upcoming numerical models, it is necessary to calibrate the results of the numerical models using accepted physical test data or case studies. In this study, two main field studies were used in simulations: The simulation of the reinforced concrete wall tested in a mine environment and the pre- and postconvergence response of a mine opening to be modeled. The model setup was calibrated through the explosion test conducted at the regarded reinforced concrete wall for the simulation of the mine environment at the field. Then, the mine environment was converted to the coal mine environment as in the case of the field where the abutment convergence data were gathered. The coal seam mechanical parameters were assigned by the parameters found from the rock mechanics experiments conducted on the samples taken from the same coal seam. Following that, the abutment simulation was applied to the models. The abutment-loaded coal mine opening with the concrete stopping has been subjected to several explosion scenarios, including single or multiple coal mine explosions.

Field Studies

Reinforced Concrete Walls

US federal regulations required seals to withstand a 20-psi (0.14 MPa) explosion pressure prior to the Sago Mine disaster in 2006. The "Sealing of Abandoned Areas; Final Rule" by Mine Safety and Health Administration (MSHA) was published on April 18, 2008, and it specifies requirements for seal strength, design, and construction (73 Fed. Reg. 21182, MSHA 2008). The Code of Federal Regulations final rule (CFR 2007) states seals must be able to withstand 50 psi (0.34 MPa) if the sealed area is monitored and kept inert, 120 psi (0.83 MPa) if it is not, or > 120 psi if certain conditions exist that could result in a higher explosion pressure. A NIOSH report (Zipf et al. 2009) presents all structural data from explosion tests performed at the Lake Lynn Experimental Mine (LLEM) on seals designed to meet the former 0.14 MPa pressure design standard between 1997 and 2008 to facilitate the analysis and design of seal structures that meet the new explosion pressure criterion. The report groups and presents the measured displacement–time ($D-t$) curves and applied loading or pressure–time ($P-t$) curves for 44 different seal structures tested before 2006, when the former 0.14 MPa explosion pressure design criterion for mine seals was in effect (Zipf et al. 2009). The response $D-t$ curves and applied loading $P-t$ curves for eight different ventilation stoppings made of solid or hollow concrete blocks are also part of this data set. The results of these structural tests conducted against the stoppings are provided as supplementary data that are important for the seals' design (Zipf et al. 2009). Six different seal construction categories, categorized by the primary seal building material and method, were tested as part of the program. The first category of these structures is made of concrete or

materials that resemble concrete, like shotcrete or gunite, with additional steel reinforcement bars that anchor to the surrounding rock and internal steel reinforcement. Only two tests on seals made of materials that resemble concrete and have internal steel reinforcement that meets the requirements for reinforced concrete seals were conducted.

The structure used in this study for calibration belongs to the *Category 1A seal* from these two structures. In this structure, steel reinforcement bars are used to anchor the seal to the surrounding strata. Insteel 3D panels, a three-dimensional welded wire space frame, are also included. The structural elements of the seal are made up of a plane of Vertical #8 reinforcement bars and #8 reinforcement bar anchors into the roof and floor in front of each panel, a plane of Horizontal #8 reinforcement bar anchors into each rib, and #3 steel reinforcement bars laid horizontally from rib to rib within the panels. Grade 60 steel is used for rebars and anchors (Fig. 1). A fast-setting concrete mixture is applied from the front side of the seal to fill the 30-cm-thick panels. Two sets of vertical holes are uniformly placed across the entry on < 60 cm centers, drilled into the roof and floor to a minimum depth of 30 cm. The vertical holes are offset between the front and back rows. Each rib has three horizontal holes bored into it, each 30 cm deep and 60 cm apart. These vertical and horizontal holes are grouted with 0.9 m long #8 steel rebar anchors. The ultimate wall measures 2.1 m in height by 5.8 m in width.

While this structure is also used in the subsequent analyses, another similar structure is investigated within this study's scope. As previously mentioned, the other structure in the recommended BIP RA design is the steel-reinforced concrete structure (Trackemas et al. 2015). In this design, the provided design example was created by adapting well-known design principles for protective structures from the "Unified Facilities Criteria (UFC): Structures to Resist the Effects of Accidental Explosions" (UFC 2008). The 15-psi (0.1 MPa) design 0.2-s P–t curve has a rise time of 0.1 s and a fall time of 0.1 s. This example design's entry measurements are 6 m wide by 2.4 m high. The thickness of this rebar-reinforced concrete wall is 30 cm. The RA stopping wall's vertical and horizontal reinforcement bars measure 3.175 cm in diameter (#5 bar) and are spaced 30 cm apart on either side. Sitrrups of 2.5 cm diameters (#4 bar) serve as shear reinforcement at the intersections of the horizontal and vertical reinforcement bars. Rock bolt anchors of 1.5 cm diameters (#5 bar) spaced every 0.45 m are used to secure the RA stopping wall to the surrounding rock. The 1.5-m-long anchors are embedded 0.6 m in the RA stopping structure and grouted 0.9-m into the nearby rock. A total of 40 rock bolt anchors are needed. This RA-stopping design for rebar-reinforced concrete is depicted in Fig. 2. These two walls are named Wall Z (designed by Zipf et al. 2009) and Wall N (designed by NIOSH researchers, Trackemas et al. 2015) throughout this paper for simplification, and the main information is summarized in Table 1.

Convergence Response

A case study (Oyler et al. 2001) was used to be simulated by numerical models for the abutment-loading of an abandoned coal

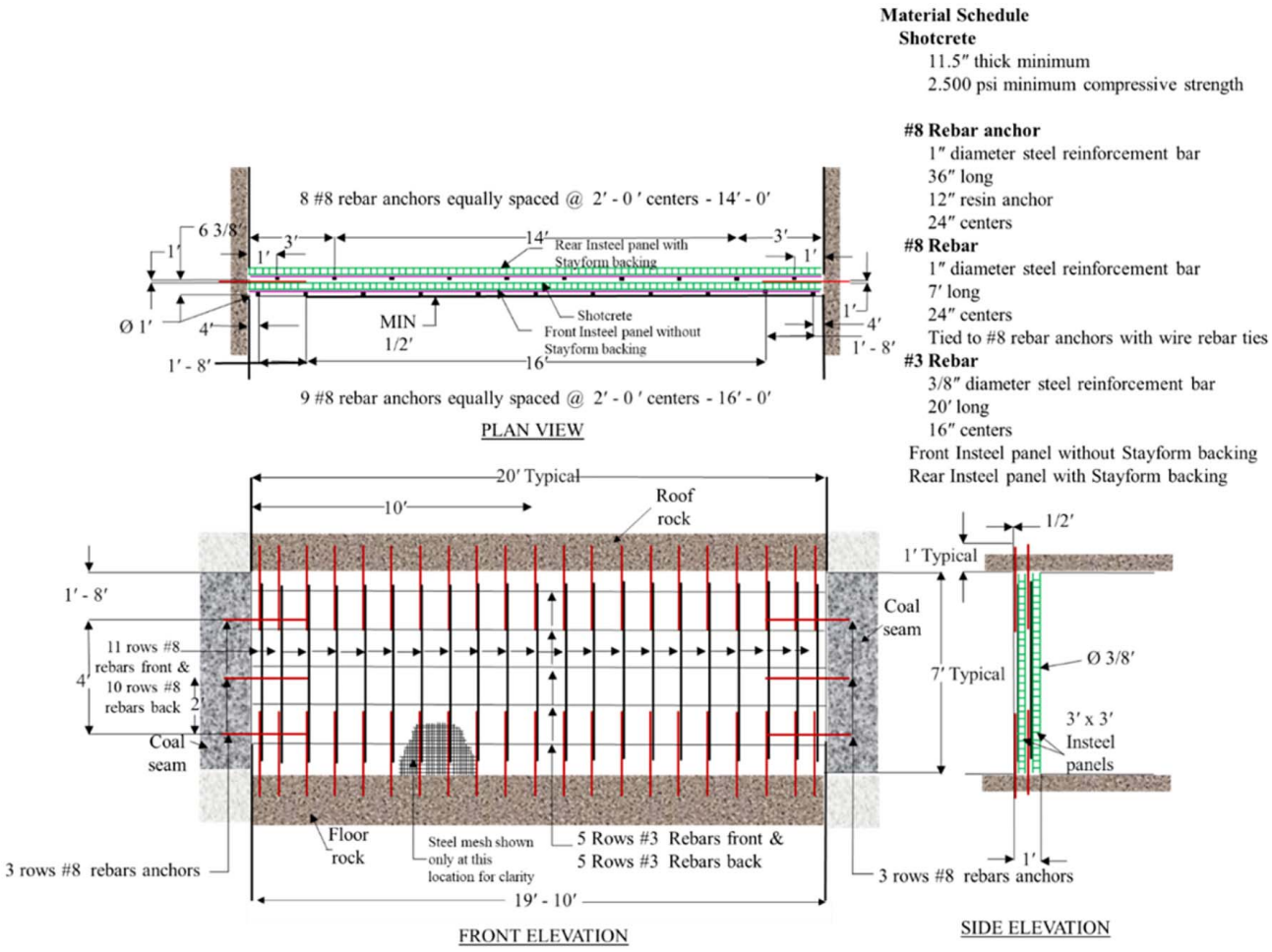

Fig. 1. Drawings of the first reinforced-concrete structure used. (Reprinted from Zipf et al. 2009.)

Int. J. Geomech., 2024, 24(6): 04024100

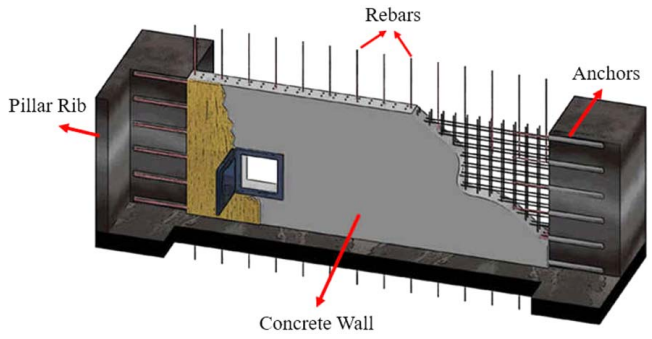

Fig. 2. Sketch of the design example for BIP-RA stopping. (Reprinted from Trackemas et al. 2015.)

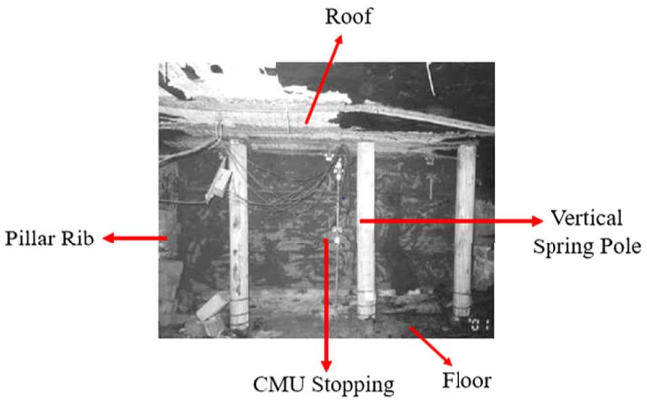

Fig. 3. View of the CMU stopping at a crosscut. (Reprinted from Oyler et al. 2001.)

mine opening with a concrete wall. This case study's investigations of underground measurements to ascertain the loading response of stoppings made of lightweight aggregate concrete masonry units (CMU) are presented. This study has yielded some intriguing findings that may be useful for developing and evaluating alternative stopping construction techniques as well as designing and choosing standard construction techniques for use in various mining conditions. The information gathered from the field study is being used to understand how concrete block ventilation stoppings react to ground movements associated with mining, particularly during longwall retreat (abutment-loading condition). The research site is in a coal mine that exploits the Pittsburgh coalbed, the thickest and most extensive coal bed in the Appalachian Basin in southwest Pennsylvania. The Pittsburgh coalbed measures about 2.1 m on average in the study area, with a 0.2 m parting and a 0.3 m upper split. Approximately 1.8 m of thinly bedded silty shale, interbedded with sandstone and sandy shale, make up the majority of the roof strata. While direct observation of the site's floor geology was not conducted, data from nearby coreholes indicate that the immediate floor consists of approximately 0.15–0.6 m of shale and fireclay, followed by a layer of 0.3–1 m of limestone and limey shale (Oyler et al. 2001).

To scrutinize the case study, four stoppings in total, two between the headgate (belt) and track entries and two between the track and (future) tailgate entries, were instrumented at the crosscuts of the mine. Two of the instrumented stoppings were built with lightweight concrete blocks being tested as alternatives, and two with lightweight aggregate CMUs that are frequently used at the mine (Oyler et al. 2001). However, owing to some unwanted problems during the project, one stopping has been replaced with a new one, and the convergence data are provided regarding this crosscut (Fig. 3).

Near the center and about 0.6 m laterally from the stopping point, a vertical spring-mounted pole with mountings for measuring roof-to-floor convergence and stopping lateral movement was used. Fig. 4 depicts the cumulative convergence of the two stoppings built into Crosscut 33. Data trends were used to estimate convergence during the 5 days following the removal of the original stopping and before the installation of instruments on the replacement stopping. Except for the Inby side sensor 11, which was estimated to have moved about 1 mm during this time, all convergence sensor locations were estimated to have converged an additional 8 mm. The face was 17 m from the crosscut's center when the original stopping was removed, and Sensors 9, 10, and 11 (outby, middle, and inby) recorded convergence rates that were roughly constant at 0.25 mm/day. The longwall face was almost at a crosscut when the replacement stopping started recording data. At that time, the convergence rates had risen to about 3 mm/day. When the face passed 41 m away from the stopping point, convergence rates started to rise quickly, with the outlying side showing a noticeably higher rate. With instantaneous convergence rates for Sensors 9, 10, and 11 of 68, 33, and 8 mm/day, respectively, convergence rates peaked when the face was roughly 60 m away from the crosscut. Once the face was 175 m outby, the rates started to rapidly decline, reaching a stopping rate of 1.5 mm/day. Convergence rates stabilized at about 0.25 mm/day when the face was 474 m away from the crosscut (roughly 2.2 times overburden depth), which was essentially the original convergence rate before the first longwall pass. Typical longwall side abutment-load and the presence of a cutter roof condition on the outby side of the crosscut, according to visual observations, are what caused the convergence across Crosscut 33 (Oyler et al. 2001). The presence of the cutter may have had an equal or more significant impact on stopping loading than the vertical loading of the pillars, based on the large difference in convergence rates on the inby and outby sides of the stopping. Therefore, the data from Sensor 11 (inby) were used in the simulations of the abutment not to take into account the effect of roof cutter.

Experimental Studies

Based on the findings in the literature (Oyler et al. 2001; Karadeniz et al. 2023), it can be concluded that geomechanical stress state of strata plays a crucial role in the responses of the stoppings. According to plate theory (Timoshenko and Woinowsky 1959), fixed-end constraints provide more resistance to plate rotation and lateral plate displacement than simply supported ends, which permit rotation at the edges. It is hypothesized that as small set loads from

Table 1. Summary of the concrete walls used in this study

Wall types used	Height (m)	Width (m)	Thickness (m)	Anchor diameter (mm)	Rebar diameter (mm)	Grade	Bar spacing (m)	Embedded length into rock (m)
Wall *Z* (Zipf et al. 2009)	2.1	5.8	0.3	4.2	2.3	60	0.6	0.3
Wall *N* (Trackemas et al. 2015)	2.4	6.0	0.3	3.1	3.1	60	0.45	0.9

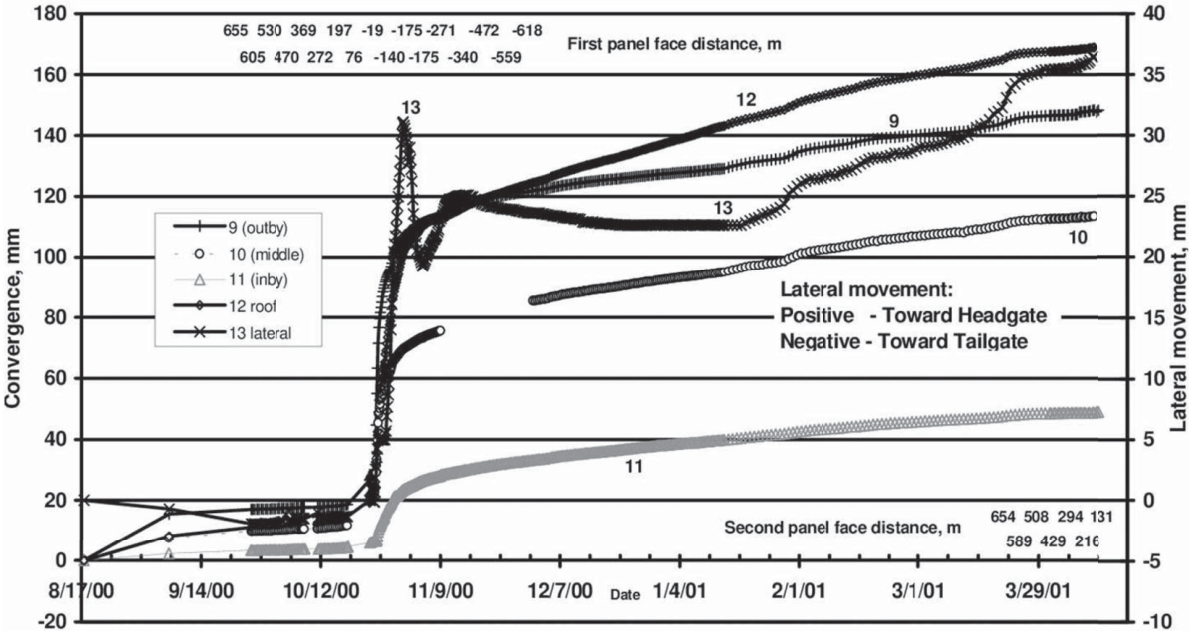

Fig. 4. Total convergence at Crosscut 33. (Reprinted from Oyler et al. 2001.)

wedges or loads caused by mine convergence are introduced, the points of contact between the stopping and the roof, rib, and floor start to behave more like fixed support as a result of increases in end-support friction and stiffness (the latter as a result of gap reduction). Blocks' resistance to sliding will also increase due to an increase in interface friction. Hence, the determination of the properties of the overlying strata material and contact parameters that encompass the physical properties and characteristics that delineate the interface between the bedding planes found within sedimentary rock strata or rock formations is very important.

Since the abutment-loading-based convergence to be simulated belongs to the Pittsburgh coal seam, the coal blocks were taken from the same field to conduct fundamental rock mechanics laboratory experiments on 50 by 50 mm cubical specimens (Fig. 5). The quantity of uniaxial compressive strength (UCS) and static deformability tests performed on each coal sample served as the foundation for this analysis. The number of UCS tests from the specified coal bed is regarded in this analysis as a representative sample of the lithotype. The UCS and Young's modulus (E) of the coal samples, along with loading direction and standard deviation, are provided in Table 2 and Appendix I, where H refers to the height of the sample, and W1 and W2 refer to the other two dimensions. Based on the experimental results of 34 samples, the input UCS and E values are determined to be 15.7 MPa and 1.5 GPa, respectively. The overlying roof and floor parameters were taken from the literature because the samples taken from the field for determining the roof and floor rock material parameters were insufficient. In the literature study used for these parameters, conducted by NIOSH, ground response curves for longwall tailgate conditions were created using numerical models of Pittsburgh coal seam geology (Barczak et al. 2008). This study displays the geological profile that was simulated in the models. The Pittsburgh Seam in Western Pennsylvania's weak shale strata with alternating weak and strong beds are overlain by the coal bed. The thick, sturdy limestone beds in the roof strata are critical to this region's lithology. The strength information used by NIOSH researchers for the various rock types included in the models was based on data for coal-measure rocks that had been published (Rusnak and Mark 1999; Zipf 2005). Based on the values provided in the literature, the roof and floor parameters were taken to be the same to simplify the roof and floor lithologies in the models. The researchers of this study found that the elastic overlying rock strata condition is the most unfavorable case for stopping response based on the previous studies and theories. Hence, to simplify the strata as one solid rock matrix, the parameters were assumed to be 9.2 GPa of bulk and 5.5 GPa of shear

Fig. 5. Representative image from the coal sample deformability and UCS tests.

Table 2. Rock mechanics laboratory results

Loading directions	UCS (MPa)	Young's modulus (MPa)
Perpendicular average	17.87	1,556
Parallel average	13.58	1,492
Perpendicular std.	5.13	428
Parallel std.	5.58	624
Average	15.7	1,525
Average std.	5.71	528

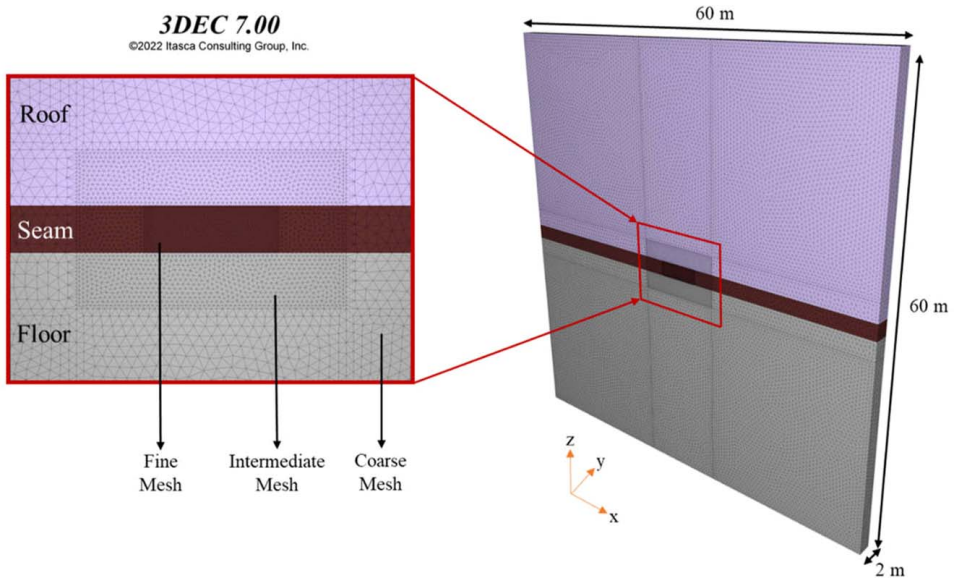

Fig. 6. Modeling geometry and discretization.

modulus with 0.25 Poisson's ratio instead of taking into account the effect of bedding planes and various lithologies.

Numerical Simulations

The ground response, reinforced concrete, and explosion loading were simulated by using the distinct element code 3DEC (Itasca 2021). With the aid of the software, it is possible to simulate the behavior of rocks in a realistic manner, from their initial elastic response to the significant displacements and deformations accompanying rock failure.

By creating 3D geometry, coal mine models with certain seam heights for two different steel-reinforced concrete stoppings were first simulated. The area of interest, influences in the discretization, and required boundary conditions were taken into consideration (Karadeniz et al. 2023). The details, such as material and joint constitutive model assignments and in situ stress initialization, will be given in the following sections. The excavation was used to make an opening in the coal seam that would serve as the crosscut for the analysis scenario. Then, using 3DEC's *block fill command*, steel-reinforced concrete models are partially placed into the excavation. After filling the excavation zone partially with the simulated wall, the mine model was subjected to the vertical loading scenario based on the convergence data used, as previously mentioned (Oyler et al. 2001), to simulate the abutment-loading. The abutment-loading simulation was achieved by increasing the model's vertical loading. According to Barczak et al. (2008), the study was conducted at the same coal seam field, and the vertical loading of the model increased by 20% and 120% for the side and face abutment stages, respectively. It will be shown in the following parts that the increased vertical loading scenarios in this study are compatible with that of Barczak et al. (2008). The models for both steel-reinforced concrete walls were subjected to various dynamic loading cases with and without abutment-loaded conditions.

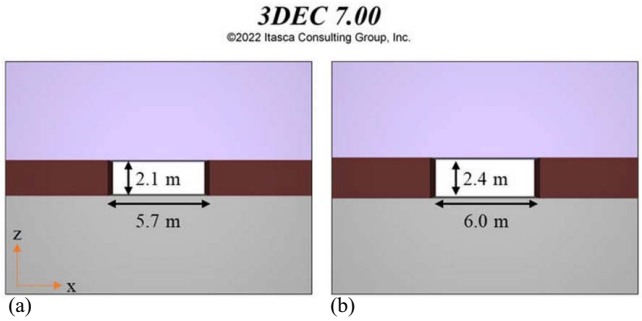

Fig. 7 Excavated crosscut simulations: (a) mine seal (reprinted from Zipf et al. 2009); and (b) BIP RA design recommendation by NIOSH (reprinted from Trackemas et al. 2015).

Model Setup

Modeling Methodology

The numerical model involves several steps, such as developing the geometry, choosing the appropriate material properties, assigning material and contact constitutive models, setting boundary conditions, initializing in situ stress, zonking for plastic models, abutment-loading, simulating the excavation and fill of the concrete wall, and dynamic loading. The development of a 3D geometry with dimensions of 60 m × 60 m × 2 in the *x*-, *z*-, and *y*-directions, respectively, allowed for the simulation of mine models with seam heights of 2.1 and 2.4 m (Fig. 6). Three different edge lengths of tetrahedral elements were used to zone the geometry; these are identified as the excavation, intermediate, and rest zones, ranging in mesh sizes from fine to coarse. Different levels of mesh sizes and tetrahedral elements were assigned to reduce the amount of time needed to solve a single model. This is because using static and dynamic time integration solutions for strata and explosion simulation results in high computational costs. The edge lengths were chosen to be 10, 20, and 50 cm to prevent abrupt change between these zones. It should be noted that preliminary models with gradually increasing mesh sizes and models run with a mesh size of 10 cm produced similar results, and boundary conditions were imposed to be fixed displacement on all sides of the model.

Previous studies (Karadeniz et al. 2023) demonstrated that assuming elastic strata for material and contact constitutive models results in more conservative explosion resistance responses on the wall. Therefore, for this study, the roof, seam, and floor were assigned an isotropic elastic constitutive model. Conversely, contacts' normal and shear stiffnesses are required inputs when using numerical modeling tools like 3DEC to simulate ground control issues. The elastic joint constitutive model was used to control the contacts that were formed between the lithologic units (the roof and seam or the seam and floor). According to Li et al. (2015), published data on the stiffness of rock joints demonstrate that normal and shear stiffnesses vary greatly, and the enormous stiffness variance significantly influences the outcome of the numerical analysis. After experimenting with a variety of inputs and comparing the results to empirical data, Esterhuizen et al. (2010) offer a set of input parameters for the numerical modeling of coal pillars that are presumptively satisfactory based on the requirements of matching the Bieniawski strength equation and obtaining identical failure depths and stress gradients as observed in the field. Although the input parameters provided cover contact friction angle, cohesion, and tensile strength with normal and shear stiffness values (100 and 50 GPa/m, respectively), the plastic material properties were not taken into account as the elastic contact constitutive relations were assigned.

In situ stresses were initialized by different approaches for the coal seam and rock layers. G. S. Esterhuizen's (personal communication, 2017) suggestions [Eqs. (1, 4, and 5)] were used to calculate the in situ stresses in the rock layers. Eqs. (1)–(3) were provided by Liu et al. (2016). The initialization of coal seam in situ stress was studied by Mohamed et al. Because Mohamed et al. (2021) used an overburden depth range of 91–320 m, and only one specific depth of 320 m was assigned to model the extremum condition in this study, the simulated mining conditions represent the typical US coal mine environments.

$$\sigma_v = \gamma \times Z \tag{1}$$

$$\sigma_{Hc} = 1.174 + 0.024 \times Z_c \tag{2}$$

$$\sigma_{hc} = 0.018 \times Z_c - 1.475 \tag{3}$$

$$\sigma_{Hr} = 0.313 + 0.027 \times Z_r + 0.000278 \times E_r \tag{4}$$

$$\sigma_{hr} = 0.65 \times \sigma_{Hr} \tag{5}$$

where Z_c and Z_r = depths of the coal seam and rock layers, in meters, respectively; and σ_v = maximum vertical stress for both the coal seam and the rock layers with the specific weight of units in (MN/m^3). σ_{Hc} and σ_{hc} are the maximum and minimum horizontal stresses. While σ_{Hr} and σ_{hr} are the maximum and minimum horizontal stresses of the rock layers, respectively, E_r is Young's modulus of the rock layers in MPa. Megapascals are used to measure all stress units.

To place the simulation of the concrete wall designs by Zipf et al. (2009) and NIOSH researchers (Trackemas et al. 2015), excavations with dimensions of 5.7 m width × 2.1 m height and 6.0 m width × 2.4 m height, respectively, were made in the coal seam to represent the crosscut (Fig. 7). After reaching the equilibrium of stress initializations, excavation was done in the models. Since the plastic models were excluded, the full excavation was applied all at once without reducing the strength of the coal in that zone.

Utilizing 3DEC's *block fill command*, steel-reinforced concrete was partially filled into the excavation. The first excavated block's entire geometry is retained in memory by the block excavate command. The block fill command replaces the original block with a new one. Because the block excavate command joins blocks, a particular procedure must be used if only a portion of the excavation is to be filled (2021). Following the excavation being filled, the blocks in the fill volume are unjoined, the model zero is cycled to create subcontact between the filled and excavated blocks, the unfilled blocks are re-excavated, and the properties of the zones and joints are checked.

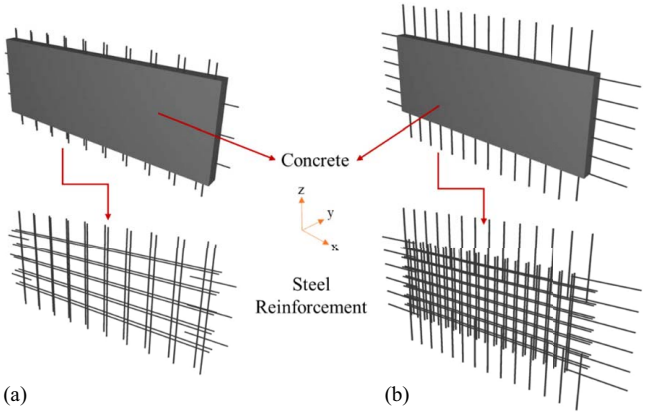

Fig. 8. Simulated steel-reinforced concrete walls: (a) mine seal (reprinted from Zipf et al. 2009); and (b) BIP RA design recommendation (reprinted from Trackemas et al. 2015).

A thorough understanding of the entire stress–strain dynamics is required to comprehend the mode of failure of concrete structures. Concrete is a heterogeneous, cohesive-frictional material that displays complex nonlinear behavior under a multiaxial stress condition. A Mohr–Coulomb strain-softening constitutive model was selected to simulate the filled zone with the geometries of 2.1 m height, 5.7 m width, and 2.4 m height, 6.0 m width, 0.30 m thickness, which corresponds to the concrete wall, as shown in Fig. 8. Density, bulk, and shear modulus, cohesion, friction angle, and tensile strength were the variables used in the model. Cohesion and tensile strength were relaxed while maintaining a constant friction angle. The concrete wall was modeled with a 50% loss of cohesiveness at 0.3% strain, a 70% loss at 0.35% strain, and a 90% loss at 0.4% strain. Postpeak tensile response of the material was simulated as 95% loss at 0.3% strain, 98% loss at 0.35% strain, and 99% loss at 0.4% strain. The seal design study by Kallu (2009) was imposed as the source for these softening parameters. Utilizing cable elements, the 3DEC model simulates the field use of the reinforcement steels. The configurations for both concrete designs in numerical simulations are as in Fig. 8.

Upon the excavation and filling of the zone to simulate the reinforced concrete wall, the contact around the excavation changed to concrete–rock interfaces. Therefore, a new joint constitutive model was assigned using the advantage of the 3DEC distinct element method. The concrete wall–rock contacts were explicitly modeled using the same methodology as Kallu (2009). The interface in Kallu's finite-element analysis was given an elastic-perfectly plastic model (Kallu 2009). The parameters used for the contacts were taken from a study on in situ shear testing of concrete–rock interfaces (Gravel et al. 2015). Considering both studies, contacts were modeled with zero cohesion and a 58° of friction angle.

The blast pressure acting on the structure is known as an impulse because explosive loading only lasts a few milliseconds.

The influence of stress wave propagation through the material is crucial in analyzing mechanical components subjected to impulsive stimulation. The stress wave will cause a change in mechanical components' stress redistribution over time, resulting in stress levels that are higher than those predicted by static loadings. The solution algorithm uses direct integration to get the temporal evolution of the displacement and stress fields. The damping is a crucial parameter in dynamic analysis because the damping in the numerical simulation should, in terms of magnitude and form, correspond to the energy losses in the natural system when subjected to dynamic loading. Rayleigh damping is frequently used in time-domain applications (Itasca 2021). There are two types of damping in 3DEC: stiffness-proportional and mass-proportional. A force opposite to the velocity that is proportional to absolute velocity and mass is exerted by mass-proportional damping. The force applied to contacts or materials in zones by stiffness-dependent damping is proportional to the stiffness matrix and the relative velocities or strain rates. In 3DEC, either type of damping can be used by itself or in tandem, known as Rayleigh damping (Bathe and Wilson 1976). A damping matrix, C, is created in dynamic finite-element analysis from components proportional to the mass (M) and stiffness (K) matrices with the mass-proportional damping constant and the stiffness-proportional damping constant, respectively. The critical damping ratio and fundamental frequency are required to define these two parameters in 3DEC. The damping of materials varies between 2% and 10%, with geological materials damping between 2% and 5% and structural systems between 2% and 10% (Biggs and Biggs 1964). In this study, the damping ratio values are assumed to be those obtained from an experimental study on concrete material (Tian et al. 2017). According to that study's experimental findings, the damping is between 1% and 6% with a signal center frequency of 20–100 kHz, satisfying the assumption of a low damping ratio. Based on that, the damping parameters used in this study were assumed to be 5% of the damping ratio with a 50 kHz center frequency.

Concrete Wall Calibration

As mentioned previously, at the Lake Lynn Experimental Mine, NIOSH performed a number of structural tests on coal mine seals and stoppings. The experiment of steel-reinforced concrete wall design in Category 1A was used in the calibration of the underground mine stoppings. It is obvious that the deformation of the concrete wall under the same dynamic loading condition exhibits different results because the strata behavior plays a crucial role in response to the stopping. As a result, to calibrate the 3DEC models in the initial models, the LLEM's boundary conditions were used. The roof, rib, and floor rocks in the LLEM are limestone with an intact compressive strength of roughly 167 MPa and an intact modulus of elasticity of roughly 66 GPa, according to laboratory studies conducted by D. R. Dolinar (personal communication, 2008). The rock mass in the LLEM is of acceptable quality, with a Rock Mass Rating (RMR_{89}) ranging from 77 to 79 (G. S. Esterhuizen, personal communication, 2008). Young's modulus was downscaled and assumed 37 GPa for rock mass with a Poisson's ratio of 0.25. The roof, rib, and floor conditions for seal structures constructed and tested in the LLEM are *rigid* or *unyielding*. Compared with underground coal mines, where the roof and floor rock, as well as the coal ribs, would be less stiff and strong, the foundation conditions for the seal tests in the LLEM are not typical (Zipf et al. 2009). The same equations [Eqs. (1, 4, and 5)] to simulate the rock in situ stress conditions for the limestone units in LLEM were used in the calibration models.

Table 3. Calibrated input parameters for concrete wall

Parameter	Value
Density (kg/m^3)	2,200
Young's modulus (GPa)	40
Poisson's ratio	0.2
Cohesion (MPa)	7
Friction angle (°)	20
Tensile strength (MPa)	3.5

To calibrate the models, the central displacement versus time plot ($D-t$) was used, and the recorded explosion pressure versus the time ($P-t$) curve (Zipf et al. 2009) was subjected to the structure. The elastic and plastic material properties attributed to the concrete structures are given in Table 3. According to several studies, concrete structures with steel wire mesh reinforcement produce a localized membrane effect and are more blast-resistant than slabs without it (Li et al. 2017; Wei et al. 2020). For the sake of model simplicity, the wire meshes were not simulated with external structural elements, but the concrete's elastic modulus (E) was increased to 40 GPa with a constant Poisson's ratio of 0.2. The tensile strength of the material, rather than any other plastic material properties, was found to be the most governing when the input parameters for the concrete wall were changed through the iterative process during the calibration.

The obtained displacement response at the center of the wall exhibits good agreement with the recorded displacement–time curve in the experiment. The residual displacement from the model has an offset of 0.5 mm, even though the magnitude of the peak displacement predicted by the model is identical to the actual amount. Fig. 9 displays the calibration of the models by plotting the measured and predicted displacement versus time and the recorded explosion pressure versus the time curve.

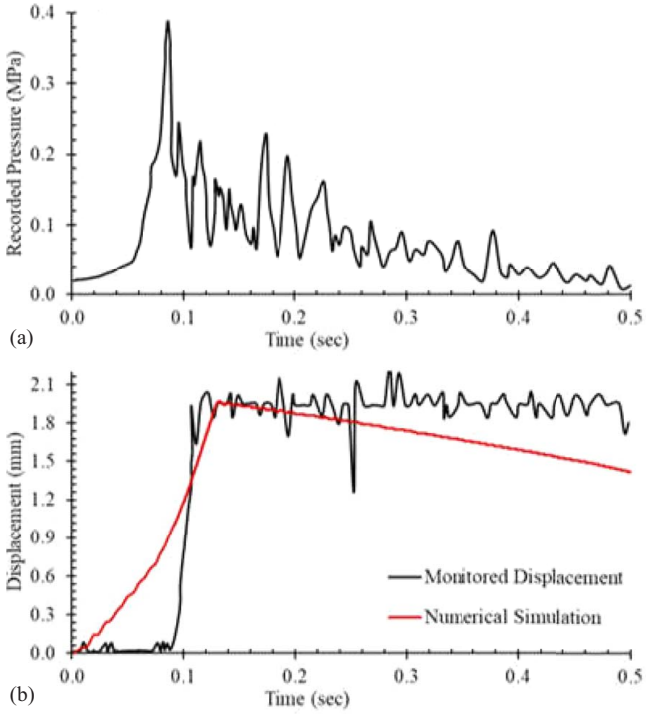

Fig. 9. Recorded (a) pressure versus time; and (b) displacement versus time curves with the numerical calibration. (Reprinted from Zipf et al. 2009.)

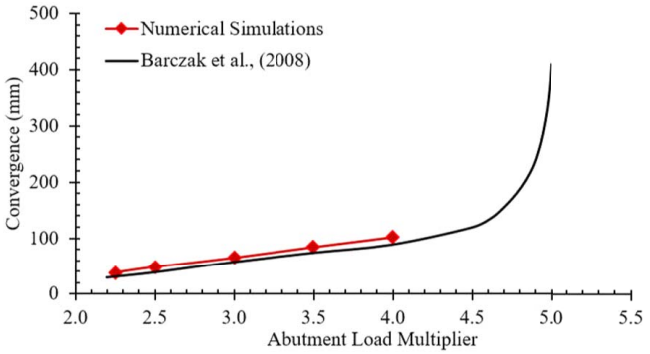

Fig. 10. Validation of the models with the convergence versus abutment-load multiplier curve. (Reprinted from Barczak et al. 2008.)

Strata Response Calibration

As stated previously, numerical models were also used to simulate the abutment-loading of a coal mine opening with a concrete wall based on a case study (Oyler et al. 2001). It was intended to implement specific levels of convergence in this study, including 5, 15, 25, 35, 40, and 50 mm. Barczak et al. (2008) simulated the abutment-loading by increasing the vertical loading of the model by 20%–120% for the side abutment and face abutment stages. In that study, from the base case of 2.2 times the overburden load to 2.5 times the overburden load, the face abutment stress was increased. It was then incrementally increased by an additional 0.5 factor, up to 5.0 times the overburden load. This is done to assess the effects of pillar yielding and deformation. With these stress multipliers, the tailgate convergence at the face location increased linearly until the factor reached 4.0. Beyond this, the convergence started to intensify more. The pillar failure was severe and the immediate roof and floor damage in the tailgate entry exceeded a stress multiplier of 4.5.

In this study, the abutment-loading was provided by applying a certain velocity from the top of the mine model to increase the vertical stress, similar to Barczak et al. (2008). Upon increasing the vertical stress, a halt rule was coded so that the displacement of the gridpoints at the specified zone could reach desired convergence levels. The zone in the numerical models is assigned similarly to the sensors placed by Oyler et al. (2001), which stood close to the center and 0.6 m laterally away from the stopping. To this halt rule, the model continues to increase the vertical load till that given average displacement level. Following that, the abutment-loaded walls are subjected to explosion simulations.

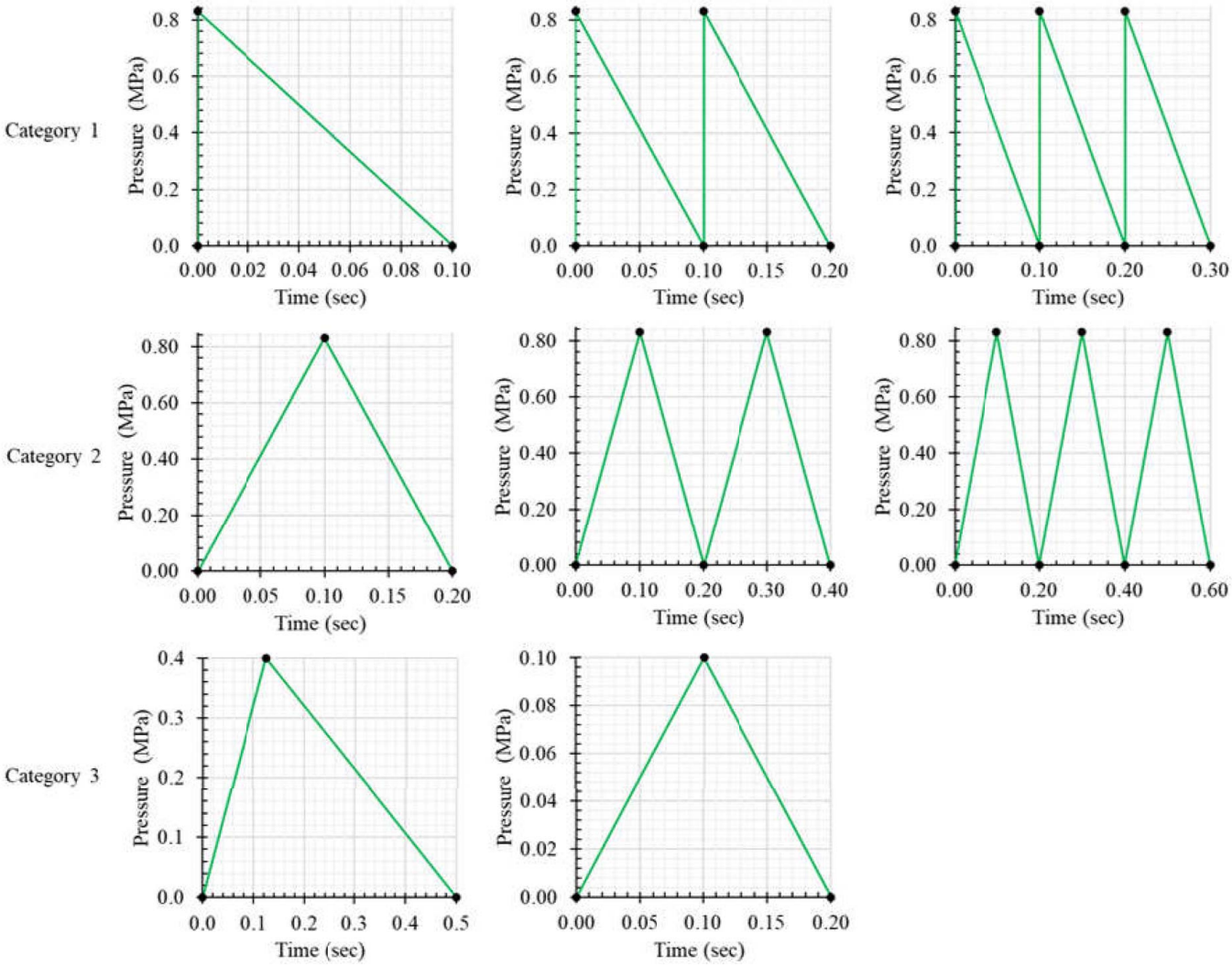

Fig. 11. Applied pressure versus time curves with their categories.

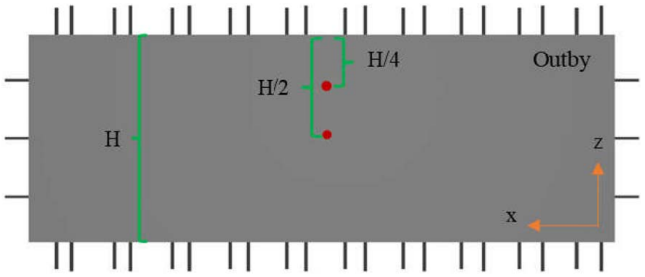

Fig. 12. Historical point representation for Wall *Z*.

To validate the vertical loading of the strata, the tailgate convergence–abutment-load multiplier curve, which Barczak et al. (2008) provided, was utilized. However, since the modeling approach of this study covers only elastic strata conditions, the linear portion of the convergence–load curve was referenced. The vertical stress increase of the models in terms of vertical stress multiplier, the ratio of the increased vertical stress to initial stress level, corresponds closely to that linear portion (Fig. 10).

Model Results and Discussion

Since the main goal of this study is to reveal the effects of wall deformation with changes in vertical loading conditions during panel extraction, it was intended to simulate particular levels of convergence, such as 5, 15, 25, 35, 40, and 50 mm. These convergence levels are coded as C5, C15, C25, C35, C40, and C50, respectively. For the explosion simulation, various dynamic loading scenarios were implemented. Eight different $P-t$ curves ranging from 0.1 MPa (15 psi) to 0.83 MPa (120 psi) explosion pressure are considered to examine the failure analysis of the stopping. Mine seals could be subjected to multiple explosions in underground coal mine situations. Various $P-t$ curves with various explosion pressures, including multiple explosion scenarios, are also chosen to study the

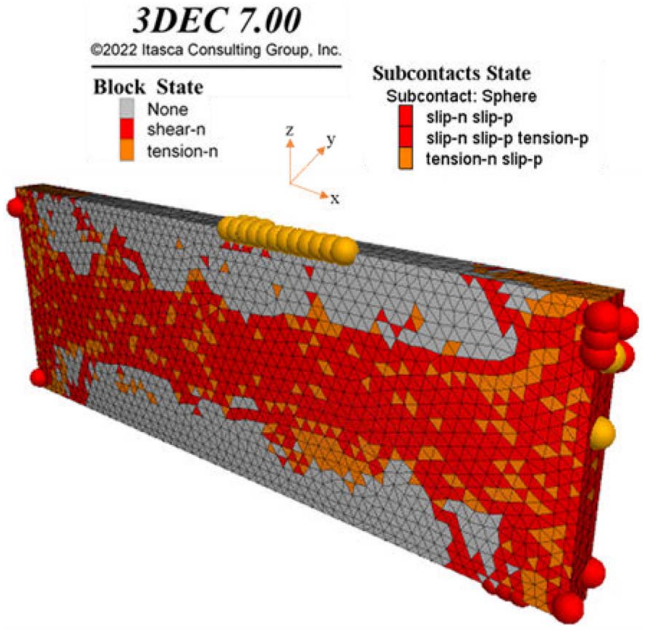

Fig. 14. Contact and element state regarding both walls at 50-mm convergence level.

reinforced concrete. One of the curves is the recorded explosion $P-t$ curve of Zipf et al. (2009), as previously presented, whereas the other one is with a magnitude of 15 psi (0.1 MPa), a rise time of 0.1 s, and a fall time of 0.1 s. The Office of Mine Safety and Health Research (OMSHR) recommends this design $P-t$ curve for RA stopping (Trackemas et al. 2015). The remaining $P-t$ curves were taken from Kallu (2009) for both single and multiple explosion scenarios. These scenarios and the two prior ones are classified into instantaneous rise time and 0.1-s downtime, 0.1-s rise and downtime with their multiple explosion versions (two and three explosions in a row), Zipf et al. (2009) recording, and

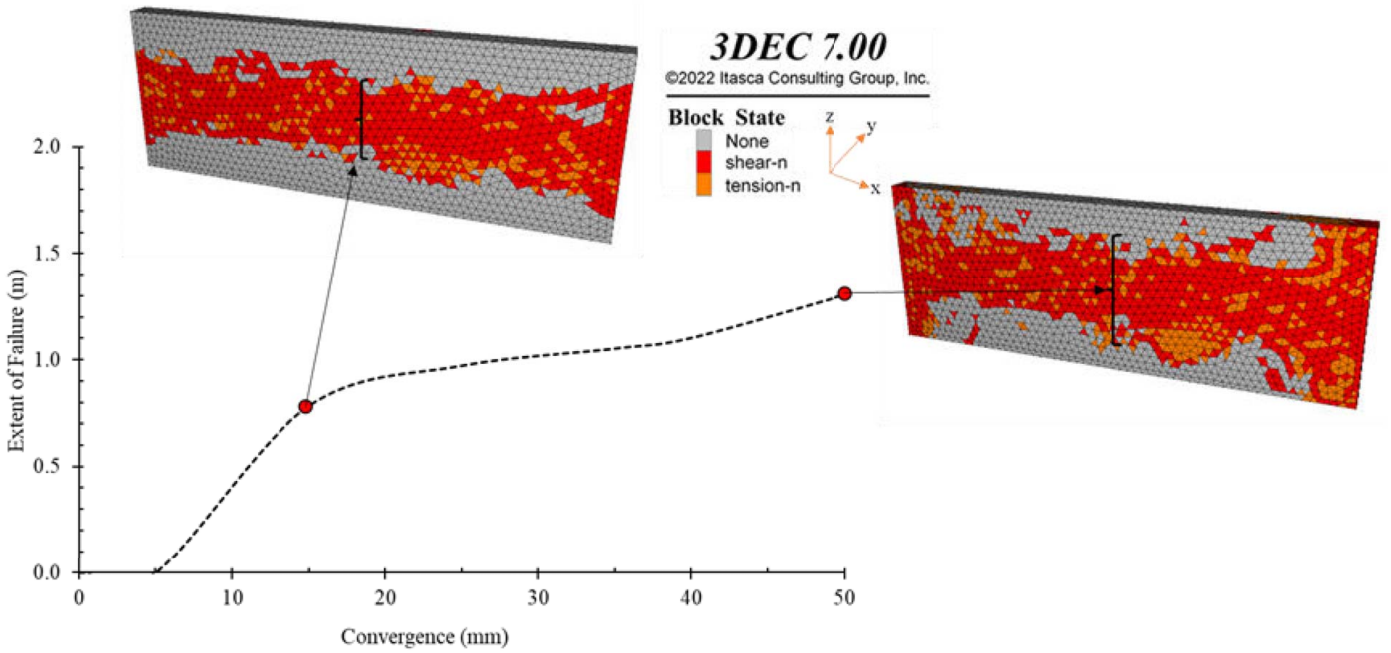

Fig. 13. Comparison of the walls subjected to abutment-loadings in terms of the extent of failures at the outby face.

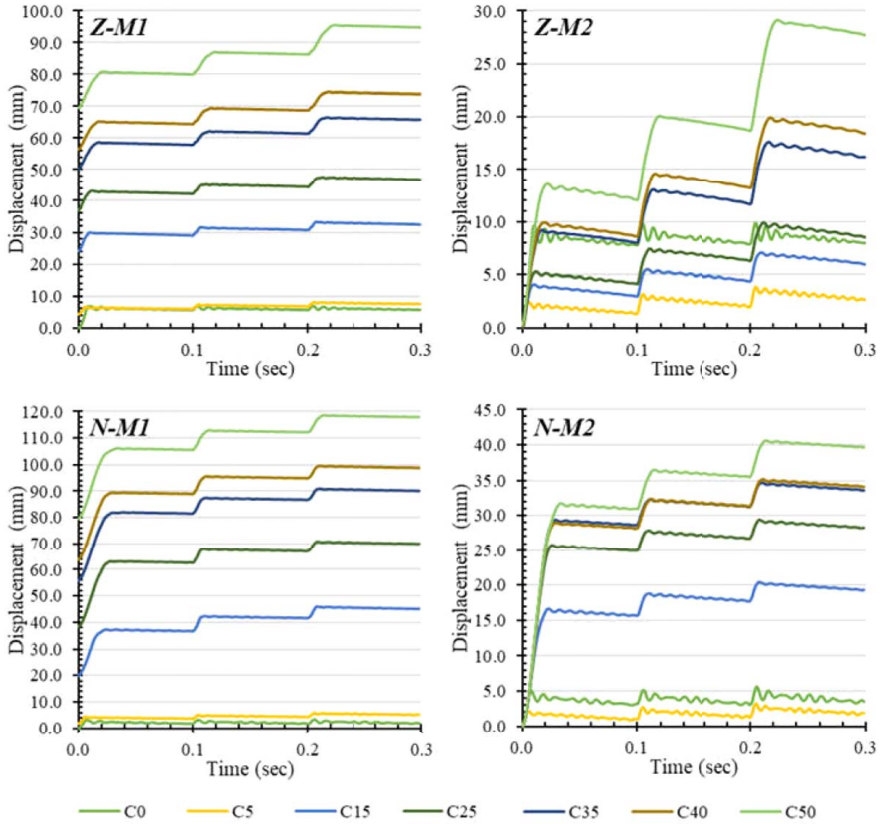

Fig. 15. Representative displacement–time curves of both walls for three explosion scenarios in Category 1.

OMSHR curve. Fig. 11 shows these eight different applied $P-t$ curves with their categories.

The deformation data on the walls were captured to present and interpret the results; further discussions will be provided as well. Since the highest deformation zone was previously known by the theory and numerical experiences, several historical points were determined, and two specific monitoring points were used, one at the center (M1) and the second at central top (M2) of the outby face of the walls. Fig. 12 shows the historical sampling representation for one of the walls. The central top historical point was located at the lateral center and vertical midpoint between the center and roof of the opening. The results are demonstrated to be a displacement versus time plot for each wall with different convergence levels (C0, C5, C15, C25, C35, C40, and C50) with their labels for the two monitoring points (M1 and M2).

The increased abutment-loading damages were studied prior to the walls being subjected to explosion loadings. The increasing vertical level results in the failure zones starting from the central portion to the upper and lower sections. These zones are initially governed by shearing failure modes and turned into tensile cracking by increased vertical stress. There are two mechanisms triggering these failures; shear failures are mainly caused by the compression of the increased vertical stress, and the other is based on the expansion of the concrete wall in the y,z-plane (displacement in "+" and "−" y-direction) with the Poisson effect. The failure mode comparison of walls is based on the vertical extent of the failed zone from the center of the walls since the responses of the structures are symmetrical. The results demonstrate that the failure analysis of both concrete walls gives similar shear failure zones; hence, the concrete failure is represented by one of the walls (Fig. 13). There are two main aspects in the steel reinforcements of the structures; the configuration inside the concrete and installation through the rock and coal seam. Although the inside configurations are different, the reinforcement densities are quite similar. The main difference is the length of the embedded steel in the overlying and underlying strata. Wall N has 90 cm of embedded steel into rock and seam, while Wall Z has 30 cm of embedded reinforcements.

Prior to the outcomes of the dynamic numerical simulation, it should be noted that NIOSH engineers chose the allowable wall rotation angle of 1° as a failure criterion for unreinforced walls with one-way arching (Zipf et al. 2007). To this criterion, the critical displacement at the center of the wall is the function of wall height and allowable rotation angle so that the displacement is equal to half of the wall height, multiplied by the tangent of that allowable rotation angle. This criterion is accepted to be the medium level of protection (Zipf et al. 2007). The primary premise of the arching analysis is that the structure is in rigid contact at the roof and floor interfaces and that displacement along these interfaces does not occur in a shear or splitting failure mode. According to this criterion, the allowable displacement at the center is 18 and 21 mm for Walls Z and N, respectively. However, there is a reason that it is not appropriate to use that measure to compare with the results presented in that study: the contacts around the concrete structure (the contact between roof, seam, and floor) yield during the explosion simulation (Fig. 14).

Category 1

For the instantaneous rise time and 0.1-s downtime explosion scenario at Wall Z, the single explosion loading exhibits displacements up to 14 and 80 mm, for Points M1 and M2,

respectively. The increase in displacement is around 10 mm for the central section by each 10-mm increase in the convergence for Wall *Z*, while it is around 2 mm for the upper zone deflection. Conversely, the displacements are up to 32 and 105 mm, for Points M1 and M2, respectively, for Wall *N*. The incremental change in displacement at M2 is very similar to Wall *Z*; however, the central zone response is quite different, so the deflections are significantly higher upon the convergence of 25 mm. By the multiple explosions in a row, for Wall *Z*, the displacements increase 10%–50% within each subsequent explosion at the upper and central zones. However, these percentile changes are around 5%–15% for Wall *N*. Fig. 15 shows representative $D-t$ curves for both walls regarding certain convergence levels with Monitoring points M1 and M2. The $D-t$ curves for the other scenarios are demonstrated in Appendix II.

Category 2

For Points M1 and M2, respectively, the single explosion loading exhibits displacements of up to 7 and 75 mm for the 0.1-s rise and downtime explosion scenarios at Wall *Z*. For every 10-mm increase in convergence for wall *Z*, the displacement is increased by approximately 10 mm for the central section while it is increased by approximately 2 mm for the upper zone deflection. Conversely, the displacements for Points M1 and M2 on Wall *N* are up to 20 and 95 mm, respectively. Although the incremental displacement change at M2 is very similar to that at Wall *Z*, the central zone's responses are very different, and as a result, the deflections are much greater upon the convergence of 25 mm with no certain gradual increase in the trend. For both wall types, the displacements at the upper zones increase by 25%–50% for the incremental changes in convergence during the multiple explosions in a row, and they show very similar increases as in the single multiple explosions.

Category 3

The interpretations of the lower-level loading scenarios exhibit that the central deflections are minor, around 0–0.4 mm. However, M2 history points for both Zipf et al. (2009) recording and RA criteria loading scenarios in both wall types show significantly higher values at the central deflections. They reach up to 80 mm of deflection and are very close to each other for both wall types and loading levels of 0.1 and 0.4 MPa.

The results show that, in addition to the magnitude, the loading mode significantly affects the wall response. If the first two categories are compared, the instantaneous rise time loading mode results in two times higher deflections at the center than 0.1 rise time loading mode for both wall types. For the deflection at the upper zone, the instantaneous rise time scenario is 25% and 30% higher for the Walls *N* and *Z*, respectively. These reveal that the instantaneous loading criteria can give more conservative measures to evaluate the performance of such walls under similar circumstances.

For the effects of subsequent second and third explosions, the single explosion deformations are more prominent so that the changes in deformation during the subsequent ones are comparatively minor with respect to the initial permanent deflections except for certain cases. This can be interpreted as that the first explosion resistance is the crucial event to assess the performance of the walls. The adjunctive cases are for Wall *Z* after a certain convergence for both loading modes. At the instantaneous loading mode, upon the convergence of 25 mm, the subsequent explosions create significant effects at the central zone of the wall. Conversely, Wall *Z* shows considerable percentile increases by the subsequent explosions at the level of 50-mm convergence. However, it should be noted that this exceptional case demonstrates deflections of < 12 mm.

These two walls exhibit different responses to the same scenarios. Several reasons can be pointed out to reveal these differences, although both are steel-reinforced concrete walls with the same thickness, material model, and parameters. These distinctions are as noted previously, first, the crosscut openings of the walls are not equal to each other; subsequently, the overlying and underlying strata behaviors are distinct due to the changes in induced stresses and also the varying steel-reinforcement configurations.

Conclusion

As indicated, it is necessary to estimate the underground coal mine stoppings' potential load from longwall abutment-loading and subsequent effects on the response of these structures during sudden explosions. Two separate steel-reinforced concrete walls to be employed in seal and BIP RA, applications were simulated in this work to analyze the performance and failure analysis under abutment-loading conditions during an explosion for a coal mine model utilizing dynamic analysis by a Distinct element code 3DEC. In the experimental investigation carried out by Zipf et al. (2009) at the NIOSH Lake Lynn Laboratory, one of the concrete walls was the simulation of a structure used among many seal tests. The second structure to be examined was NIOSH's BIP RA design example (Trackemas et al. 2015). The major goal of this study was to use various convergence levels to implement the impacts of wall deformation with changes in vertical loading conditions using panel extraction. This study also compared the explosion resistances of two different reinforced concrete wall models and identified quantitative changes in the deformation of the concrete walls after various explosions. Therefore, the Pittsburgh coal seam was represented by the model of a coal mine. The quantitative research of convergence experienced by longwall stoppings was used to model the abutment-loading conditions, with the data provided by Oyler et al. (2001).

Several explosion scenarios, including single or multiple coal mine explosions, have been tested on the abutment-loaded coal mine opening with the concrete stopping. Various dynamic loading situations were incorporated for the explosion simulation. Eight different $P-t$ curves ranging from 0.1 MPa (15 psi) to 0.83 MPa (120 psi) explosion pressure are taken into consideration to examine the failure analysis of the stopping.

Prior to being subjected to explosion loadings, these walls suffered damage from the increased abutment-loading. As the abutment-loading rises, failure zones appear, moving from the top to the center and lower regions. Shear failures are initially the dominant failure mechanism in these zones, but as vertical stress increases, the tensile failure mechanism starts governing the entire failure of the structure. Two different mechanisms cause these failures; the first is the expansion of the concrete wall in the y,z-plane (displacement in the "+" and "−" y-directions) due to the Poisson effect. The compression of the increased vertical stress primarily causes shear failures.

The findings also demonstrate that, in addition to the magnitude, the pressure versus time loading mode significantly affects the wall response. For both types of walls, the instantaneous rise time loading mode causes two times greater central deflections than the 0.1 rise time loading type. The instantaneous loading criterion can

provide more cautious measurements to assess how well such walls perform in similar situations. The single-explosion deformations are more pronounced than the consequences of the second and third explosions; therefore, with certain exceptions, the permanent deflections during subsequent explosions are relatively small compared with the initial.

The findings of this study can be used as a preliminary reference to understand the behavior of reinforced concrete structures under abutment-loading conditions in underground coal mines. However, it is recommended that such structures be tested in a laboratory or field scale to understand and quantify the damage at the upper zone further. Because it is highly challenging to conduct a series of explosion tests at a laboratory or field, an axially loaded reinforced structure can be subjected to a certain static load to simulate an equivalent dynamic load to capture the response under abutment and explosion loading physically rather than numerically. Upon these efforts, reinforcement recommendations can be proposed for the yielded zones on the structures due to abutment-loading.

Appendix I. Rock Mechanics Experimental Results

The coal sample's UCS and Young's modulus, along with information about loading direction and standard deviation, can be found in Table 4. In this context, "*H*" represents the sample's height, while *W1* and *W2* correspond to the other two dimensions.

Table 4. Rock mechanics laboratory results with the sample dimensions and loading orientations

ID	H (mm)	W1 (mm)	W2 (mm)	W/H	UCS (MPa)	Young's modulus (MPa)	Loading direction wrt. bedding plane
D-1	50.11	50.43	55.58	1.06	4.07	381	Parallel
D-2	54.40	43.00	62.50	0.97	7.72	946	Perpendicular
D-3	60.90	49.55	32.45	0.67	3.64	573	Parallel
D-4	51.84	63.88	60.77	1.20	12.54	1,129	Perpendicular
D-5	57.15	58.06	62.46	1.05	16.83	1,383	Perpendicular
D-6	56.33	62.61	64.48	1.13	23.54	1,956	Perpendicular
D-7	54.54	58.10	74.42	1.21	19.94	1,659	Parallel
D-8	55.31	55.24	56.93	1.01	16.85	920	Perpendicular
D-9	51.63	53.58	53.66	1.04	17.15	1,671	Parallel
D-10	48.55	54.15	61.02	1.19	21.32	1,857	Perpendicular
D-11	68.27	49.67	52.66	0.75	19.98	1,982	Parallel
D-12	55.30	54.29	46.76	0.91	14.50	1,381	Perpendicular
D-13	52.57	50.99	51.38	0.97	17.31	1,689	Parallel
D-14	66.26	67.05	68.44	1.02	10.35	1,268	Parallel
D-15	66.49	63.76	56.52	0.90	8.07	1,000	Parallel
D-16	51.51	56.69	60.59	1.14	13.71	1,105	Perpendicular
D-17	58.71	50.85	54.77	0.90	23.07	2,134	Perpendicular
D-18	50.06	58.33	58.32	1.17	16.29	1,410	Parallel
D-19	60.93	66.94	47.47	0.94	20.98	2,271	Perpendicular
D-20	48.05	68.27	38.74	1.11	8.04	1,029	Parallel
D-21	57.65	59.08	58.50	1.02	23.44	1,987	Parallel
D-22	56.41	47.10	38.20	0.76	11.74	1,112	Parallel
D-23	53.40	58.70	60.60	1.12	13.04	782	Parallel
D-24	56.34	60.70	58.78	1.06	25.83	1,970	Perpendicular
D-25	57.50	66.60	65.08	1.15	15.88	1,625	Perpendicular
D-26	64.92	68.30	76.70	1.12	26.53	2,097	Perpendicular
D-27	66.00	51.98	53.30	0.80	17.84	1,821	Parallel
D-28	47.09	46.50	58.50	1.11	18.10	1,620	Perpendicular
D-29	63.03	61.84	60.96	0.97	18.59	1,391	Perpendicular
D-30	61.80	55.29	56.70	0.91	14.46	2,634	Parallel
D-31	51.95	55.69	52.10	1.04	12.68	1,250	Perpendicular
D-32	60.04	50.56	53.59	0.87	12.11	2,095	Parallel
D-33	53.13	52.88	48.20	0.95	13.36	2,281	Parallel
D-34	48.18	48.40	38.90	0.91	15.10	1,430	Perpendicular

Appendix II. Displacement–Time (*D*−*t*) Curves for Both Walls

The figures in the paper illustrate characteristic *D*−*t* (displacement–time) curves for both walls concerning specific convergence levels, with Monitoring points M1 and M2. The *D*−*t* curves for alternative scenarios can be found in Figs. 16–22.

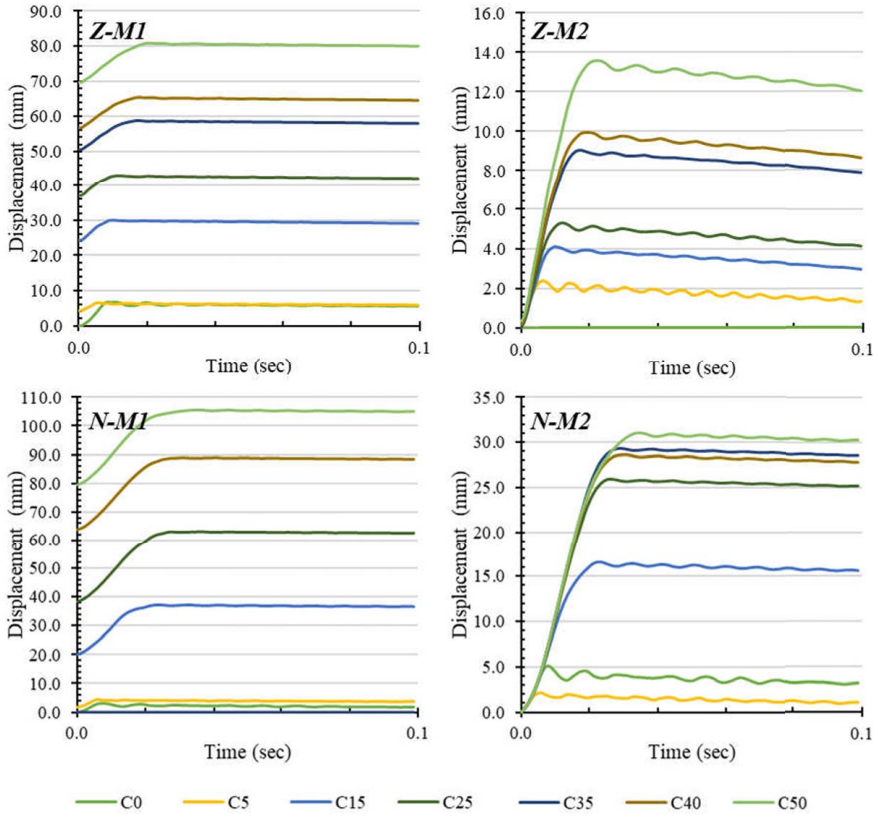

Fig. 16. Displacement–time curves of both walls for a single explosion scenario in Category 1.

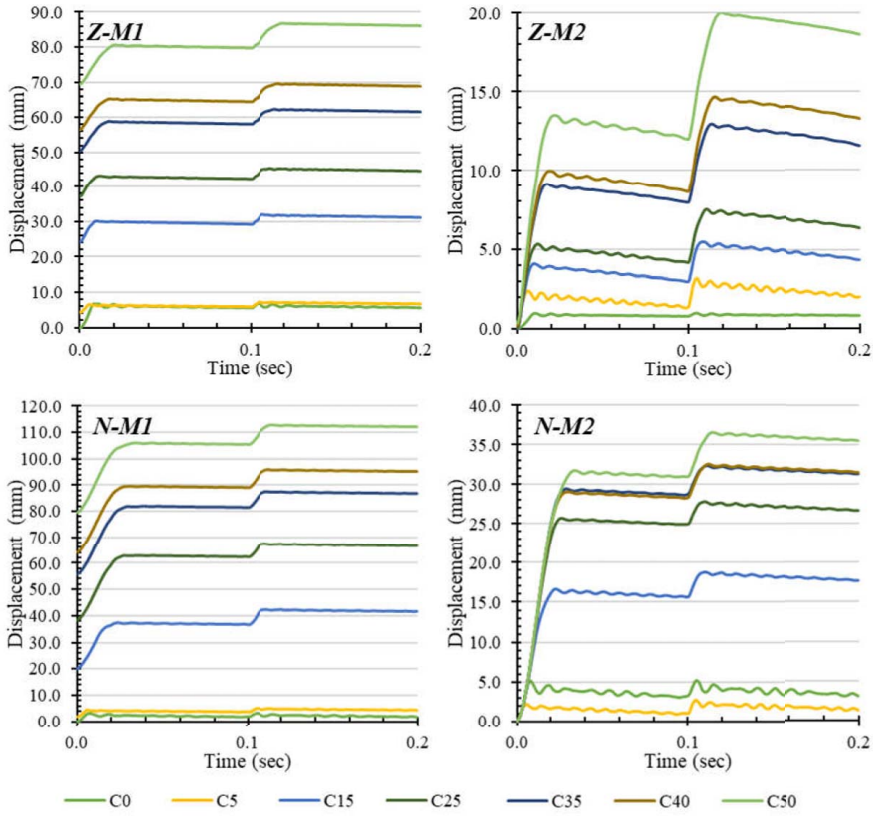

Fig. 17. Displacement–time curves of both walls for two explosion scenarios in Category 1.

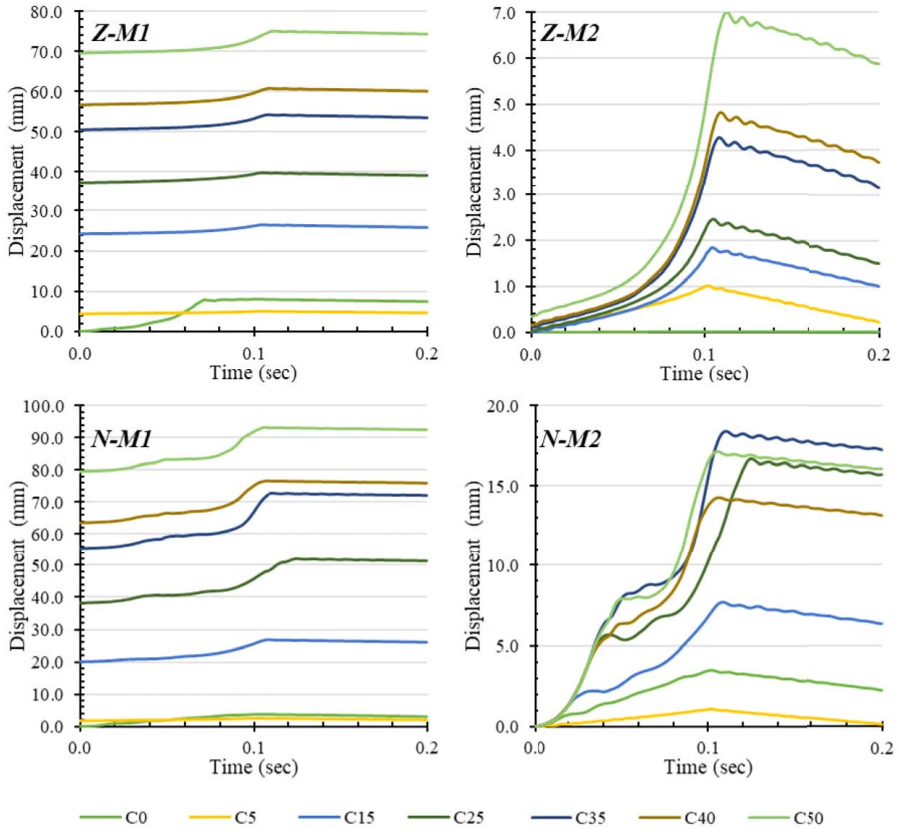

Fig. 18. Displacement–time curves of both walls for a single explosion scenario in Category 2.

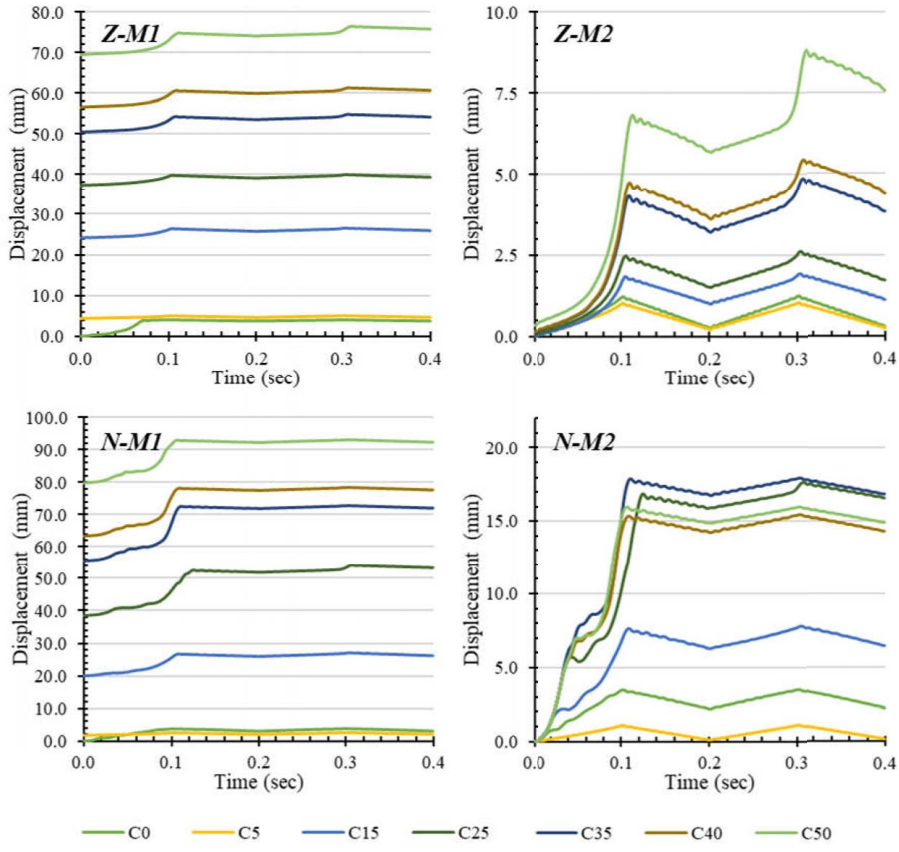

Fig. 19. Displacement–time curves of both walls for two explosion scenarios in Category 2.

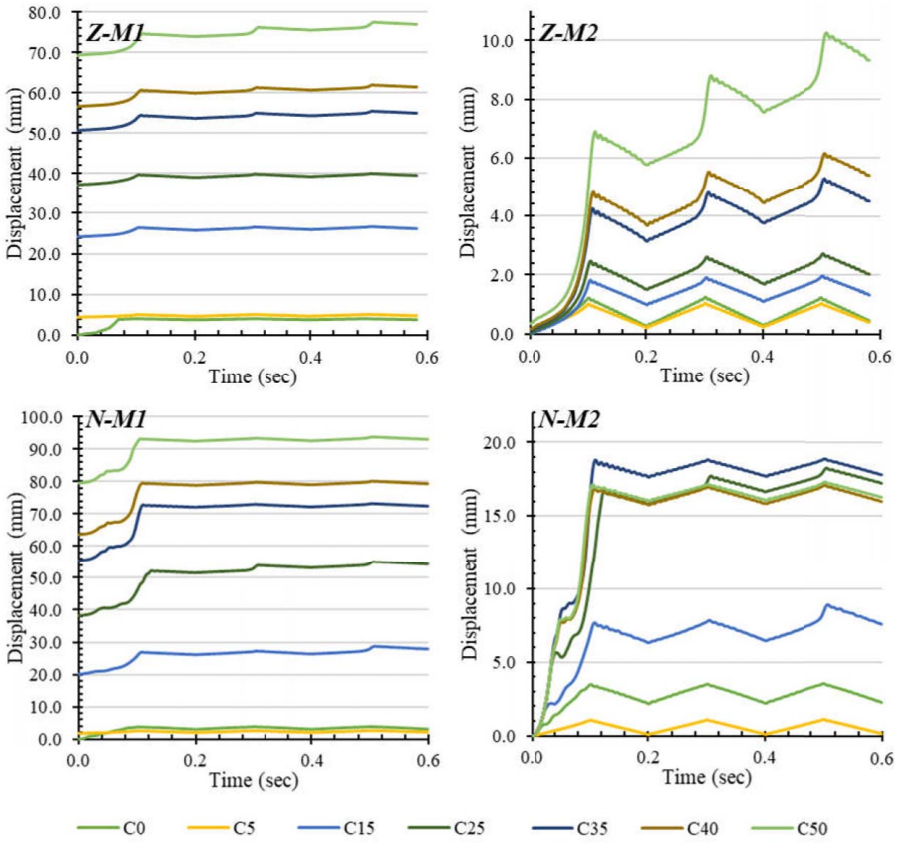

Fig. 20. Displacement–time curves of both walls for three explosion scenarios in Category 2.

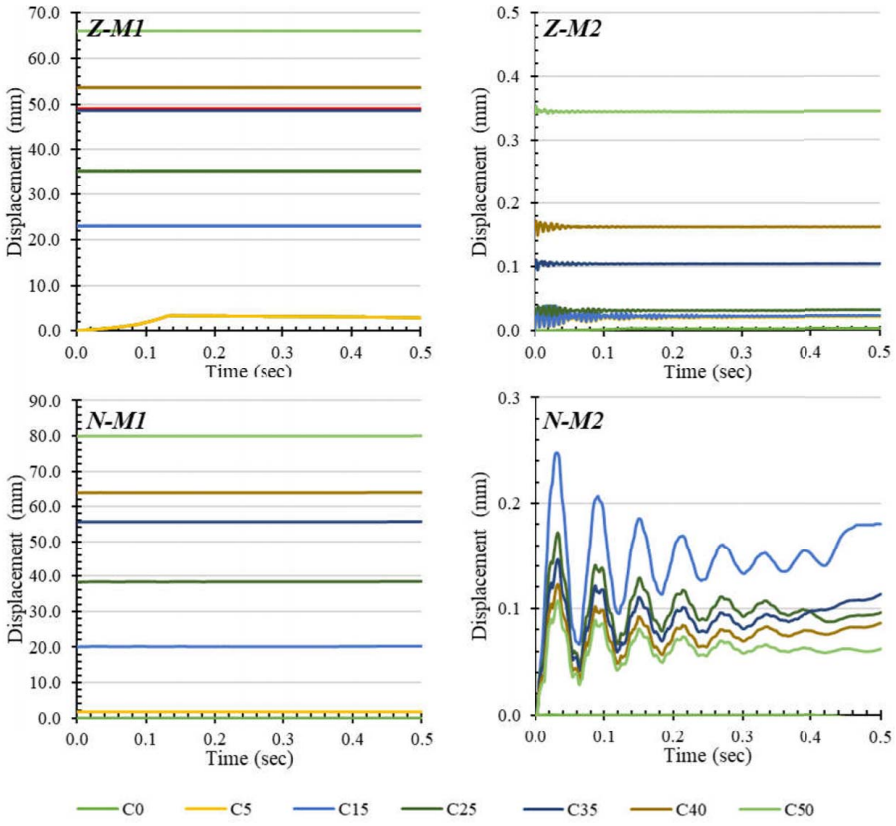

Fig. 21. Displacement–time curves of both walls for the recorded pressure–time curve. (Reprinted from Zipf et al. 2009.)

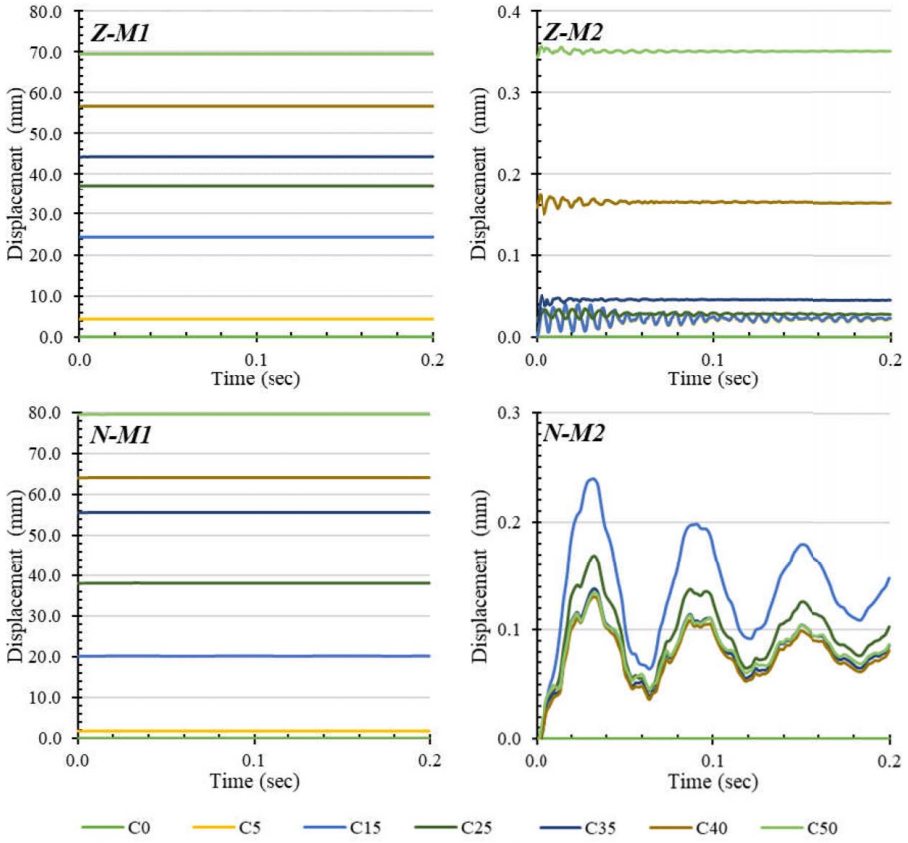

Fig. 22. Displacement–time curves of both walls for the RA criteria curve.

Data Availability Statement

All data, models, or codes that support the findings of this study are available from the corresponding author upon reasonable request.

Acknowledgments

The authors would like to thank the National Institute for Occupational Safety and Health (NIOSH), CDC-NIOSH BAA 75D301-20-R-67922, for financial support.

References

Barczak, T. M., G. S. Esterhuizen, J. Ellenberger, and P. Zhang. 2008. "A first step in developing standing roof support design criteria based on ground reaction data for Pittsburgh seam longwall tailgate support." In *Proc., 27th Int. Conf. on Ground Control in Mining*, 349–359. Englewood, CO: Society for Mining, Metallurgy & Exploration (SME).

Bathe, K. J., and E. L. Wilson. 1976. *Numerical method in finite element analysis*. Englewood Cliffs, NJ: Prentice-Hall.

Biggs, J. M., and J. Biggs. 1964. *Introduction to structural dynamics*. New York: McGraw-Hill College.

Borg, A., B. P. Husted, and O. Nja. 2014. "The concept of validation of numerical models for consequence analysis." *Reliab. Eng. Syst. Saf.* 125: 36–45. https://doi.org/10.1016/j.ress.2013.09.009.

CFR (Code of Federal Regulations). 2007. *(30 CFR 75.335(a))*. Washington, DC: US Government Printing Office, Office of the Federal Register.

Chen, L., Q. Ou, Z. Peng, Y. Wang, Y. Chen, and Y. Tian. 2022. "Numerical simulation of abnormal roof water-inrush mechanism in mining under unconsolidated aquifer based on overburden dynamic damage." *Eng. Fail. Anal.* 133: 106005. https://doi.org/10.1016/j.engfailanal.2021.106005.

Esterhuizen, G. S., C. Mark, and M. M. Murphy. 2010. "Numerical model calibration for simulating coal pillars, gob, and overburden response." In *Proc., 29th Int. Conf. on Ground Control in Mining*, 46–57. Englewood, CO: Society for Mining, Metallurgy & Exploration (SME).

Gai, Q., Y. Gao, L. Huang, X. Shen, and Y. Li. 2023. "Microseismic response difference and failure analysis of roof and floor strata under dynamic load impact." *Eng. Fail. Anal.* 143: 106874. https://doi.org/10.1016/j.engfailanal.2022.106874.

Gallagher, R. 2005. "Research needs in regard to design, performance criteria, construction, maintenance assessment and repair of coal mine seals." In *Proc., 2005 Coal Operators' Conf., Mining Engineering*. Carlton, Australia: The Australasian Institute of Mining and Metallurgy.

Gravel, C., Z. Moradian, A. Fathi, G. Ballivy, P. Rivard, and M. Quirion. 2015. "In situ shear testing of simulated dam concrete–rock interfaces." In *Proc., 13th ISRM Int. Congress of Rock Mechanics*. Montreal, QC: Canadian Institute of Mining, Metallurgy & Petroleum.

Humphries, P. 1999. "Newlands underground spontaneous combustion monitoring and management." In *Proc., 1999 Queensland Mining Industry Health and Safety Conf.*, 218–225. Townsville, Australia: Queensland Mining Council.

Itasca Consulting Group. 2021. *3DEC ver. 7.0*. Minneapolis: Itasca.

Kallu, R. R. 2009. *Design of reinforced concrete seals for underground coal mines*. Morgantown, WV: West Virginia Univ.

Karadeniz, K. E., S. Nowak, D. Guner, and T. Sherizadeh. 2022. "Evaluation on underground refuge alternatives and explosion survivability: A review." *Min. Metall. Explor.* 39 (6): 2311–2331. https://doi.org/10.1007/s42461-022-00682-1.

Karadeniz, K. E., S. Nowak, D. Guner, and T. Sherizadeh. 2023. "Dynamic response analysis of a reinforced concrete structure in underground coal mine environment with various strata conditions." *Min. Metall. Explor.* 40 (2): 563–581. https://doi.org/10.1007/s42461-023-00737-x.

Li, J., C. Wu, H. Hao, and Y. Su. 2017. "Experimental and numerical study on steel wire mesh reinforced concrete slab under contact explosion." *Mater. Des.* 116: 77–91. https://doi.org/10.1016/j.matdes.2016.11.098.

Li, W., J. Bai, J. Cheng, S. Peng, and H. Liu. 2015. "Determination of coal–rock interface strength by laboratory direct shear tests under constant normal load." *Int. J. Rock Mech. Min. Sci.* 77: 60–67. https://doi.org/10.1016/j.ijrmms.2015.03.033.

Liu, H., S. Sang, J. Xue, G. Wang, H. Xu, B. Ren, C. Liu, and S. Liu. 2016. "Characteristics of an in situ stress field and its control on coal fractures and coal permeability in the Gucheng block, southern Qinshui Basin, China." *J. Nat. Gas Sci. Eng.* 36: 1130–1139. https://doi.org/10.1016/j.jngse.2016.03.024.

Mark, C. 1990. Vol. 9247 of *Pillar design methods for longwall mining*. Pittsburgh, PA: US Dept. of the Interior, Bureau of Mines.

Mark, C. 2006. "The evolution of intelligent coal pillar design: 1981–2006." In *Proc., 25th Int. Conf. on Ground Control in Mining*, 325–334. Englewood, CO: Society for Mining, Metallurgy & Exploration (SME).

Michael, S., and V. Mutton. 2017. "The case for developing an Australian technical specification for structural design of ventilation control devices." In *Proc., 2017 Coal Operators' Conf*. Carlton, Australia: The Australasian Institute of Mining and Metallurgy.

Mohamed, K., M. Van Dyke, G. Rashed, M. M. Sears, and R. Kimutis. 2021. "Preliminary rib support requirements for solid coal ribs using a coal pillar rib rating (CPRR)." *Int. J. Min. Sci. Technol.* 31 (1): 15–22. https://doi.org/10.1016/j.ijmst.2020.12.006.

Mutton, V., and M. Salu. 2013. "Full scale explosion testing and design of gypsum plaster ventilation seals." In *Proc., Underground Coal Operators Conf., UOW*. Carlton, Australia: The Australasian Institute of Mining and Metallurgy.

MSHA (Mine Safety and Health Administration). 2008. *Sealing of abandoned areas; final rule*. 73 Fed. Reg. 21182. 30 CFR part 75. Arlington, VA: MSHA.

Ning, J., S. Yang, T. Ma, and X. Xu. 2022. "Fragment behavior of concrete slab subjected to blast loading." *Eng. Fail. Anal.* 138: 106370. https://doi.org/10.1016/j.engfailanal.2022.106370.

Oyler, D. C., G. Hasenfus, and G. M. Molinda. 2001. "Load and deflection response of ventilation stoppings to longwall abutment-loading—A case study." In *Proc., 20th Int. Conf. on Ground Control in Mining*, 34–41. Englewood, CO: Society for Mining, Metallurgy & Exploration (SME).

Rusnak, J. A., and C. Mark. 1999. "Using the point load test to determine the uniaxial compressive strength of coal measure rock." In *Proc., 19th Int. Conf. on Ground Control in Mining*, 362–371. Englewood, CO: Society for Mining, Metallurgy & Exploration (SME).

Sapko, M. J., E. S. Weiss, and S. P. Harteis. 2005. "Methods for evaluating explosion resistant ventilation structures." In *Proc., 8th Int. Mine Ventilation Congress*. Carlton, Australia: The Australasian Institute of Mining and Metallurgy.

Tian, Z., L. Huo, W. Gao, H. Li, and G. Song. 2017. "Modeling of the attenuation of stress waves in concrete based on the Rayleigh damping model using time-reversal and PZT transducers." *Smart Mater. Struct.* 26 (10): 105030. https://doi.org/10.1088/1361-665X/aa80c2.

Timoshenko, S., and K. S. Woinowsky. 1959. *Theory of plates and shells*. New York: McGraw-Hill Book Company.

Trackemas, J. D., E. D. Thimons, E. R. Bauer, M. J. Sapko, R. Karl Zipf, Jr., J. Schall, E. Rubinstein, G. L. Finfinger, L. D. Patts, and N. LaBranche. 2015. *Facilitating the use of built-in-place refuge alternatives in mines*. Rep. of Investigations (National Institute for Occupational Safety and Health); 9698. DHHS publication; no. (NIOSH) 2015-114. Washington, DC: NIOSH.

UFC (Unified Facilities Criteria). 2008. "Structures to resist the effects of accidental explosions." UFC 3-340-02. Dept. of Defense, United States of America, 1,943. Accessed May 6, 2023.. http://www.wbdg.org/ccb/DOD/UFC/ufc_3_340_02.pdf.

Verne, S. M., M. Salu, M. Johnston, and C. Mans. 2012. "Design and construction of water holding bulkheads at Xstratacoal's Oaky No 1 Mine." In *Proc., 2012 Coal Operators' Conf*. Carlton, Australia: The Australasian Institute of Mining and Metallurgy.

Wei, J., J. Li, and C. Wu. 2020. "Behaviour of hollow-core and steel wire mesh reinforced ultra-high performance concrete columns under lateral impact loading." *Int. J. Impact Eng.* 146: 103726. https://doi.org/10.1016/j.ijimpeng.2020.103726.

Zipf, R. K. 2005. "Failure mechanics in multiple seam mining interactions." In *Proc., 24th Int. Conf. on Ground Control in Mining*, 93–106. Englewood, CO: Society for Mining, Metallurgy & Exploration (SME).

Zipf, R. K., M. J. Sapko, and J. F. Brune. 2007. *Explosion pressure design criteria for new seals in US coal mines*. US Dept. of HHS, NIOSH IC, 9500. Pittsburgh, PA: US Dept. of HHS, National Institute for Occupational Safety and Health.

Zipf, R. K., E. S. Weiss, S. P. Harteis, and M. J. Sapko. 2009. *Compendium of structural testing data for 20-psi coal mine seals*. Information circular (National Institute for Occupational Safety and Health); IC 9515. DHHS publication; no. (NIOSH) 2009-151. Washington, DC: NIOSH.